ACS Photonics

Letter

Cite This: ACS Photonics XXXX, XXX, XXX−XXX

pubs.acs.org/journal/apchd5

Improving Indistinguishability of Single Photons from Colloidal Quantum Dots Using Nanocavities

Abhi Saxena,[†] Yueyang Chen,[†] Albert Ryou,[†] Carlos G. Sevilla,[§] Peipeng Xu,[†,∥,⊥] and Arka Majumdar*[,†,‡]

[†]Electrical and Computer Engineering, University of Washington, Seattle, Washington 98195, United States

[‡]Department of Physics, University of Washington, Seattle, Washington 98195, United States

[§]School of Natural Science, Hampshire College, Amherst, Massachusetts 01002, United States

[∥]Laboratory of Infrared Materials and Devices, Advanced Technology Research Institute, Ningbo University, Ningbo 315211, China

[⊥]Key Laboratory of Photoelectric Detection Materials and Devices of Zhejiang Province, Ningbo, 315211, China

Supporting Information

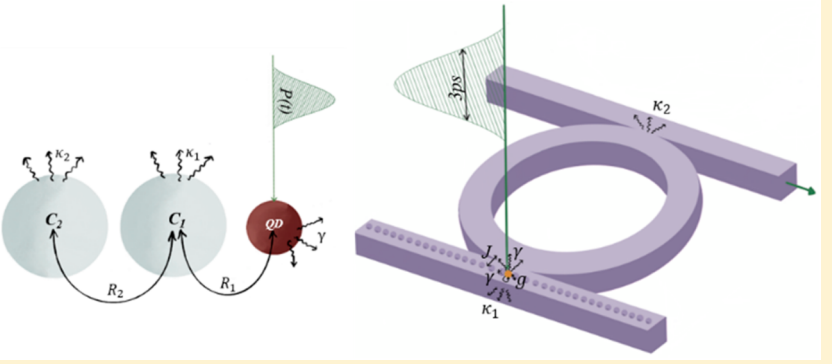

ABSTRACT: Colloidal quantum dots have garnered active research interest as quantum emitters due to their robust synthesis process and straightforward integration with nanophotonic platforms. However, obtaining indistinguishable photons from the colloidal quantum dots at room temperature is fundamentally challenging because they suffer from an extremely large dephasing rate. Here we propose an experimentally feasible method of obtaining indistinguishable single photons from an incoherently pumped solution-processed colloidal quantum dot coupled to a system of nanocavities. We show that by coupling a colloidal quantum dot to a pair of silicon nitride cavities, we can obtain comparable performance of a single photon source from colloidal quantum dots as other leading quantum emitters like defect centers and self-assembled quantum dots.

KEYWORDS: *indistinguishable single photon source, colloidal quantum dots*

Hybrid quantum photonic integrated circuits[1,2] are a promising platform to develop various quantum technologies, including universal quantum computing,[3,4] quantum networks,[5] and boson sampling.[6] A fundamental building block of this hybrid quantum photonic platform is an on-chip source of indistinguishable single photons. Quantum emitters, including self-assembled quantum dots (QDs) and single defect centers coupled to integrated nanocavities, have recently attracted significant attention as indistinguishable single photon sources due to their on-demand and high-rate single photon generation capabilities.[7,8] The indistinguishability of these solid-state emitters, which is largely limited by dephasing, is mitigated by using an optical cavity in these systems.[9] Unfortunately, none of these has been shown to maintain indistinguishability of generated single photons on a scalable platform which is a prerequisite for most quantum technologies. Solution-processed colloidal QDs can potentially provide a promising solution to this problem due to their low-cost chemical synthesis and straightforward deposition to most substrates in a scalable manner. In fact, deterministic positioning of colloidal QDs on silicon nitride (SiN) integrated photonic platform has been recently demonstrated.[10] However, despite the ease of scalable fabrication, solution-processed colloidal QDs suffer from a large dephasing rate ($\gamma^* \approx 10^5\gamma$, γ^* being the pure dephasing rate and γ being the QD dipole decay rate) at room temperature, making them unattractive as an indistinguishable single-photon source.

In this paper, we report an architecture consisting of a colloidal QD coupled to two nanophotonic resonators that improves the indistinguishability of single photons while maintaining a moderate efficiency at room temperature. Specifically, we show that our architecture can achieve comparable efficiency and indistinguishability of single photons

Received: October 10, 2019
Published: November 15, 2019

DOI: 10.1021/acsphotonics.9b01481
ACS Photonics XXXX, XXX, XXX−XXX

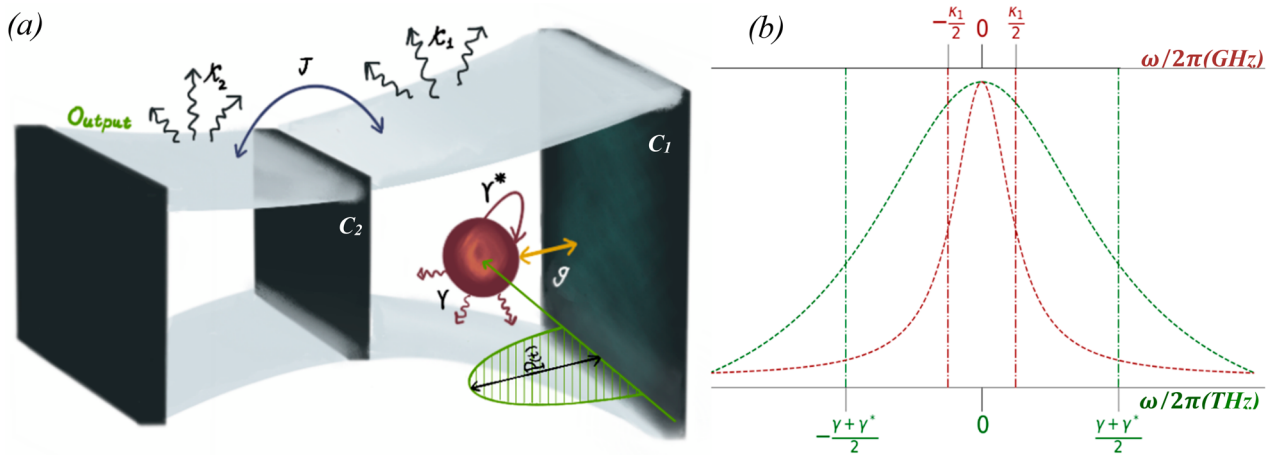

Figure 1. System description. (a) Quantum emitter with radiative decay rate γ and pure dephasing rate γ^* is coupled to an optical cavity C_1 with coupling rate g. The cavity has a decay rate of κ_1 and is coupled to another cavity C_2 with a coupling rate J. The second cavity C_2 loses photons at a decay rate of κ_2, which are collected as the output of the system. The emitter is excited incoherently through a pump pulse of amplitude $P(t)$. (b) Superimposed spectra ($\omega_o = 0$) of the quantum emitter (green) and the bare optical cavity C_1 (red) plotted on two differently scaled axes. Line width of emitter $\gamma + \gamma^* \gg \kappa_{1,2}$; the line widths of the cavities in our system, $\kappa_1/2\pi = 7.9$ GHz, $\gamma/2\pi = 0.2$ GHz, $\gamma^*/2\pi = 17.4$ THz, $Q_1 = 6 \times 10^4$, $\omega_o/2\pi = 476$ THz..

from colloidal QDs even though they suffer from order of magnitude greater dephasing than quantum emitters like silicon vacancy (SiV) centers.[11] We theoretically analyze the parameter space of our nanophotonic architecture to identify regions of high indistinguishability and efficiency. Finally, we propose an experimentally viable system to implement the architecture under the constraints of current nanofabrication technology required to obtain indistinguishable single photons from colloidal QDs. We note that our proposed method is inspired by recent work on improving indistinguishability of single photons emitted by SiV center using cascaded cavities.[11]

INDISTINGUISHABLE PHOTONS FROM BROAD DISSIPATIVE EMITTERS

For quantum emitters with a large dephasing rate, the indistinguishability I of emitted photons is given by[12,13]

$$I = \frac{\gamma}{\gamma + \gamma^*}$$

where γ is the radiative decay rate and γ^* is the pure dephasing rate of the quantum emitter. For solid and colloidal state quantum emitters at room temperatures, constantly varying local environmental conditions cause γ^* to be much larger than γ.[14,15] This effect is particularly severe for colloidal QDs, where $\gamma^* \approx 10^5\gamma$, and the indistinguishability I comes out to be $\sim 10^{-5}$, making it impossible to use the bare emitter as a useful indistinguishable single photon source.

For comparatively less dissipative emitters ($\gamma^* \lesssim 10^3\gamma$), such as single self-assembled QDs or defect centers, regions of high indistinguishability based on different mitigating techniques have been theoretically identified including: cavity-funneling of indistinguishable photons in dielectric systems,[13] usage of ultrasmall mode volume cavity to boost indistinguishability primarily in plasmonic, systems[16] or using a cascaded cavity system to get highly indistinguishable photons.[11] However, no reports exist for improving indistinguishability of emitted photons from strongly dissipative emitters like solution-processed colloidal QDs.

Our proposed system consists of two coupled cavities C_1 and C_2 and a colloidal QD pumped with a picosecond pulse, as shown in Figure 1a. Cavity C_1 has a decay rate of κ_1 and is coupled to the emitter with coupling rate g. The second cavity C_2 decays at a rate of κ_2 and is coupled to C_1 with a coupling rate of J. The photons lost by C_2 are collected as the output of the system. We can see from Figure 1b that the line width of the quantum emitter, $\gamma + \gamma^*$, is much broader than the line widths of the bare cavities κ_1 and κ_2 under consideration because of the huge dephasing experienced by the emitter.

Our system is governed by the Hamiltonian (setting $\hbar = 1$)

$$H = \omega_e e^\dagger e + \omega_{c_1} c_1^\dagger c_1 + \omega_{c_2} c_2^\dagger c_2 + g(e^\dagger c_1 + e c_1^\dagger) + J(c_1^\dagger c_2 + c_1 c_2^\dagger)$$

where $e^\dagger$, $c_1^\dagger$, and $c_2^\dagger$ are the creation operators for the emitter and the cavities C_1 and C_2 respectively.

The system dynamics is given by the evolution of the density matrix according to the master equation[17,18]

$$\frac{\partial \rho}{\partial t} = -i[H, \rho(t)] + \sum_n \left[\frac{1}{2}(2A_n \rho(t) A_n^\dagger - \rho(t) A_n^\dagger A_n - A_n^\dagger A_n \rho(t))\right]$$

where A_n denotes the collapse operators required to model the system: $\sqrt{\kappa_1}\, c_1$, $\sqrt{\kappa_2}\, c_2$, $\sqrt{\gamma}\, e$, $\sqrt{\gamma^*}\, e^\dagger e$, $\sqrt{P(t)}\, e^\dagger$, where the last term represents incoherent pumping of the QD. The collapse operator for incoherent pumping $\sqrt{P(t)}\, e^\dagger$ is time-dependent to denote a Gaussian pulse used to excite the emitter. $P(t)$ is given by

$$P(t) = P_o e^{-(t-t_o)^2/2\sigma^2}, \quad P_o = 120\gamma$$

where σ is the standard deviation corresponding to the width of the Gaussian pulse centered at t_o. We emphasize that the previous works[11,13,16] modeled the single photon source by assuming an initially excited emitter, which is strictly valid, only for resonant excitation. In most experiments, however, the single photons are generated under above-band pumping, and hence, in our model, we explicitly incorporated the incoherent pumping of the emitter using a pulsed laser. The system Hamiltonian remains the same for both the incoherent pumping and the case of an initially excited emitter, and the difference appears only in the collapse operators needed to model the system using the master equation. We note that under above-band excitation all sorts of higher energy emitter

DOI: 10.1021/acsphotonics.9b01481
ACS Photonics XXXX, XXX, XXX−XXX

states are populated, which can lead to different emitter lifetimes. The change in lifetime varies depending on the energy structures of the emitter, which are often difficult to model. To account for these nonidealities from a two-level system, the decay rate used for the colloidal QD is extracted from data measured under incoherent excitation of the colloidal QD. We point out that, in colloidal QDs, unlike the self-assembled QDs,[19] the experimentally measured Purcell factor matches very well with the theoretical predictions.[10] Therefore, the effect of the higher order states in the emitter lifetime can be neglected in our system.

The indistinguishability of photons emitted by the C_2 can be calculated as[13]

$$I = \frac{\int_0^\infty dt \int_0^\infty d\tau |\langle c_2^\dagger(t+\tau)c_2(t)\rangle|^2}{\int_0^\infty dt \int_0^\infty d\tau \langle c_2^\dagger(t)c_2(t)\rangle\langle c_2^\dagger(t+\tau)c_2(t+\tau)\rangle}$$

We can define the efficiency β of the system as the number of photons emitted by C_2, which is given by

$$\beta = \kappa_2 \int_0^\infty \langle c_2{}^\dagger(t)c_2(t)\rangle dt$$

We calculate both of these quantities via quantum regression theorem using QuTiP.[20]

PARAMETER STUDY OF INDISTINGUISHABILITY AND EFFICIENCY

In this section, we study how indistinguishability I and efficiency β vary with Q_2 (quality factor of C_2) and J (coupling between the cavities C_1 and C_2), which are our primary degrees of freedom during the design process, as well as being the key parameters in determining the system performance. We pump our emitter, a colloidal QD, with a 3 ps Gaussian pulse centered at t_o = 5 ps and calculate I and β as we move across the parameter space in order to identify regions of high indistinguishability and moderate efficiency.

To gain a physically intuitive understanding behind calculated values of I and β we study the population dynamics of the system. Qualitatively, we can break down the sequence of events that generates single photons as follows (Figure 2). Before the incoherent excitation pulse hits the emitter, the emitter is in the ground state and the cavities are empty. When the pulse hits the emitter, the population of the emitter rises at rate $P(t)$, while simultaneously decaying at rate γ and getting dephased at a rate of γ^*. Meanwhile, the cavity C_1 experiences a spike in its population, the magnitude of which depends on g, before its population decays back to zero with a decay rate of κ_1. The population in the second cavity C_2 also experiences a period of rise due to cavity coupling rate J, followed by an eventual decline to the ground state as the cavity emits photons and decays at rate κ_2. We collect these photons emitted by cavity C_2 and we want these to be as indistinguishable as possible while still being collected at practical collection efficiencies. By adiabatically eliminating the coherences in the optical Bloch equations describing the system (see Supporting Information), we define R_1 as the bidirectional population transfer rate between emitter and first cavity C_1, and R_2 as the bidirectional population transfer rate between the two cavities C_1 and C_2 (Figure 2). These are given by[11,13,21]

$$R_1 = \frac{4g^2}{\gamma + \gamma^* + \kappa_1}, \quad R_2 = \frac{4J^2}{R_1 + \kappa_1 + \kappa_2}$$

Note that such an elimination of system coherences confines us to a regime of weakly coupled cavities.

In Figure 3a,b, we calculate I and β using the master equation and plot them as a function of Q_2 (or $\kappa_2 = \omega_o/Q_2$). We consider a system with $Q_1 = 6 \times 10^4$ and $J = 2.1\gamma$ and sweep across Q_2 for four different mode volumes (V_{eff}) of C_1. The coupling strength g is inversely proportional to the $\sqrt{V_{eff}}$, whereas R_1 varies monotonically with g. In Figure 3c, we plot how R_2 changes as we sweep across κ_2.

We divide the plots in Figure 3a,c into two regions based on the relative value of $\kappa_2(Q_2)$ with respect to $\kappa_1(Q_1)$. In Region 1, where $\kappa_2 < \kappa_1$, that is, the light storage time in the second cavity C_2 is larger than the first cavity C_1, the cavity C_1 gets populated with rate R_1 from the emitter, and acts like an emitter itself for the cavity C_2. C_2 then funnels the emission into its line width, and consequently, we see a high I that increases with a decreasing κ_2 or increasing Q_2. However, in Region 2, where $\kappa_2 > \kappa_1$, this funneling cannot happen efficiently and I rapidly falls. As this process is boosted by an increased R_1, we expect I to increase with an increasing R_1. This analysis is valid when there is a dominant unidirectional flow of single photons from QD toward C_2 (Figure 2), which dictates $R_2 \lesssim \kappa_2$ and $R_1 \lesssim \kappa_1 + R_2$. This ensures that photons do not incoherently hop back and forth between C_1 and C_2 or between the emitter and C_1 at rates that are higher than the rate of loss κ_2 from C_2.

As we increase Q_2 or decrease κ_2, we expect the efficiency β to increase as we are increasing R_2, the rate of transfer to C_2 (Figure 3b). This indeed happens until a decreasing κ_2 starts becoming comparable to R_2 (shaded region in Figure 3b,c), after which instead of photons being collected at output through C_2, they are returned to C_1 at a faster rate, which lowers the β. This leads to the nonmonotonic behavior of the efficiency as a function of Q_2. Next, we look at the effect of R_1 on β as Q_2 is varied. For the system to emit with a nonzero β, R_1 must be greater than γ, because if $R_1 < \gamma$, most of the photons will be lost by the emitter itself without being transferred to the cavities leading to extremely low β values. Nonetheless, as we increase R_1, R_2 decreases, and due to this inverse relationship, β varies nonmonotonically with V_{eff} or R_1 (Figure 3b). A large enough R_1 is required to ensure that C_1 is populated, so that a transfer to C_2 can happen. But an

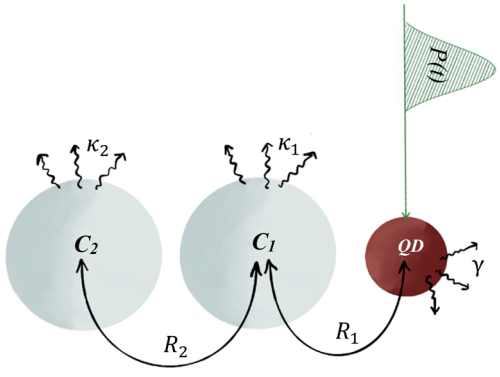

Figure 2. System schematic for population dynamics. The colloidal QD which has a radiative decay rate γ is pumped with an inchoerent pulse $P(t)$. The population transfer between the colloidal QD and C_1 occurs with a rate R_1. C_1 has a decay rate of κ_1. Population transfer rate between C_1 and C_2 is R_2. C_2 decays with a rate κ_2.

DOI: 10.1021/acsphotonics.9b01481
ACS Photonics XXXX, XXX, XXX−XXX

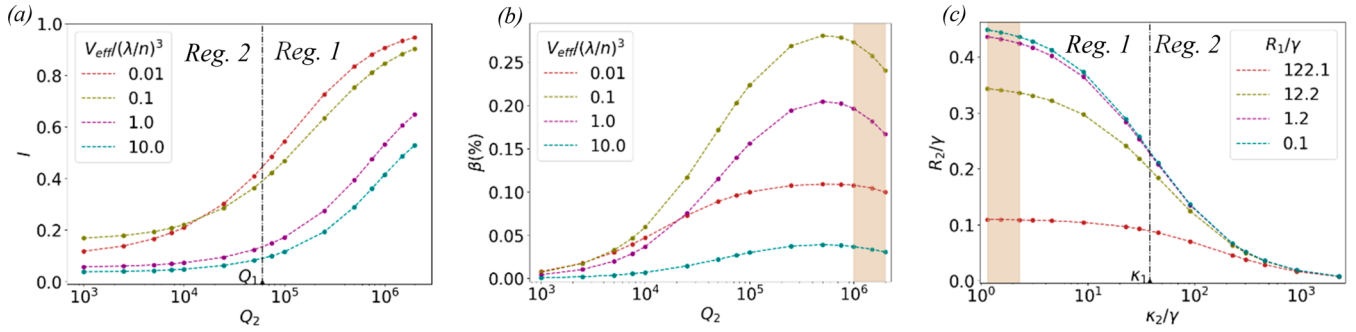

Figure 3. Parameter study of indistinguishability I and efficiency β. Each figure has four plots corresponding to four different mode volumes of the first cavity C_1, which corresponds to four different g's and, hence, four different R_1's. (a) I as a function of $Q_2(\kappa_2)$. (b) β as a function of $Q_2(\kappa_2)$. (c) R_2 as a function of $\kappa_2(Q_2)$. The figures (a) and (c) are divided into two regions depending on the relative value of $\kappa_2(Q_2)$ with respect to $\kappa_1(Q_1)$. In Region 1, $\kappa_2 < \kappa_1$, and in Region 2, $\kappa_2 > \kappa_1$. The shaded areas in (b) and (c) denote the region where κ_2 starts becoming comparable to R_2. Here, $Q_1 = 6 \times 10^4$, $J = 2.1\gamma$.

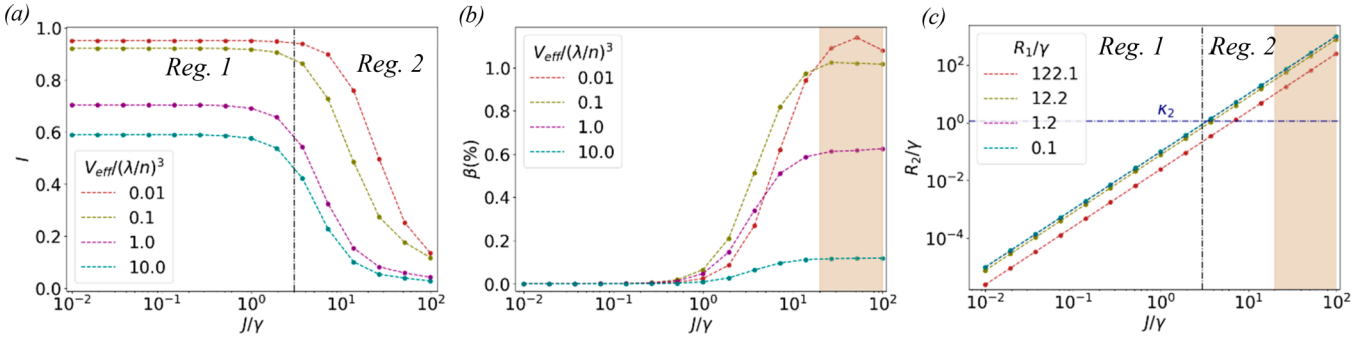

Figure 4. Parameter study of indistinguishability I and efficiency β. Each figure has four plots corresponding to four different mode volumes of the first cavity C_1 which corresponds to four different g's and, hence, four different R_1's. (a) I as a function of J. (b) β as a function of J. (c) R_2 as a function of J. Here $Q_1 = 6 \times 10^4$ and $Q_2 = 2 \times 10^6$. The figures (a) and (c) are divided into two regions depending on the relative value of R_2 with respect to κ_2. In Region 1, $R_2 < \kappa_2$, and in Region 2, $R_2 > \kappa_2$. The shaded area in (b) and (c) denotes the region where $R_2 \gtrsim R_1$.

increased R_1 also leads to a lower R_2 and, hence, an efficiency maximum exists at an intermediate value of R_1 or correspondingly V_{eff}.

To get a better understanding of I and β, in Figure 4a,b, we plot how I and β change with J, keeping $Q_1 = 6 \times 10^4$ and $Q_2 = 2 \times 10^6$ constant for four different V_{eff} or g values. Value of Q_2 is chosen such to ensure we can reach high I values as we vary J. In Figure 4c, we plot how R_2 changes when we sweep across J in Figure 4a,b.

We first analyze the plots in Figure 4a. With the help of Figure 4c, we deconstruct the figure into two regions: Region 1, where $R_2 < \kappa_2$, and Region 2, where $R_2 > \kappa_2$. In Region 1, where $R_2 < \kappa_2$, as we increase J, R_2 increases without having any significant effect on I. This happens because in this region our system is operating like the Region 1 described in Figure 3a, with cavity C_2 funneling the acquired photons from C_1 into a narrow region as it emits them. As κ_2 is held constant, I does not change significantly. The curves are arranged in an order of increasing R_1 similarly. A significant change happens in the Region 2, where $R_2 > \kappa_2$. In this region, J has become significantly large to dominate the rate dynamics, which causes the photons to incoherently go back and forth between the two cavities at much higher rates than the emission rate of C_2, and this leads to a rapid decrease in I.

Finally, we consider Figure 4b. Changing J affects R_2 only, keeping R_1 unchanged. When $J < \gamma$, R_2 is very small, and we find that β is virtually zero because hardly any population transfer occurs between the cavities. As J increases, R_2 also increases, leading to an increase in β. In Figure 3b, we observed that β varied nonmonotonically with R_1. However, now when J becomes large enough that $R_2 \gtrsim R_1$, denoted by the shaded area in Figure 4b,c, we observe that an increasing R_1 leads to an increasing β. This is because now the limiting factor on β is not the rate of transfer from C_1 to C_2, which is huge, but rather C_1 getting populated in the first place. Note that, despite high internal rates of transfer, the overall magnitude of β is still small because it is limited by κ_2, which is constant in this case and much smaller than R_2 when J becomes large.

From this analysis, we can find the optimal region of operation for our system. We need a high Q_2 and low J to ensure that emitted photons from C_2 have high indistinguishability. This, however, restricts us to operate in the region of low efficiency. There exists a trade-off between the indistinguishability and the efficiency in this region, with the optimal point of operation at J just larger than γ, where indistinguishability has not dropped significantly, but the efficiency too rises to a moderate value. Further, in this region, we can maximize the efficiency by choosing V_{eff} between $0.1\left(\frac{\lambda}{n}\right)^3$ to $1\left(\frac{\lambda}{n}\right)^3$ with lower mode volumes preferred as they lead to a higher indistinguishability.

Lastly, we would like to point to a couple of important concepts regarding the analysis of the proposed device system. First, in this device, the two cavities are only weakly coupled. Hence, the population transfer between the cavities happens due to weak coupling and the emitter is coupled only to the mode in C_1. This is fundamentally different from a system of two strongly coupled cavities where the splitting (J) is greater

DOI: 10.1021/acsphotonics.9b01481
ACS Photonics XXXX, XXX, XXX−XXX

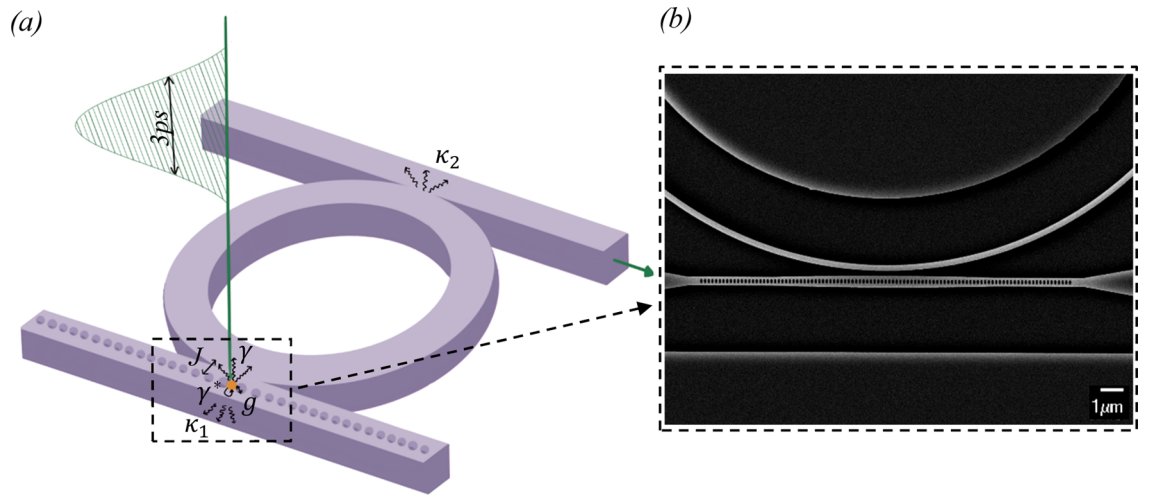

Figure 5. Experimental design. (a) Design schematic depicting colloidal QD with decay rate γ and dephasing rate γ^* coupled to the nanobeam cavity with a coupling rate of g. The nanobeam cavity has a decay rate κ_1 and is coupled to a ring resonator with a coupling rate J. The ring resonator has a decay rate of κ_2. The QD is excited by a 3 ps wide pulse with an amplitude of $P_o = 120\gamma$. The output is collected from the waveguide coupled to the ring resonator. (b) SEM image of a fabricated device structure inside the dotted black box shown in (a).

than individual cavity decay rates, and the emitter would have coupled to hybridized modes. Second, the changes in indistinguishability in the desired regime, as well as the regime of low indistinguishability in Figures 3 and 4, occur due to modified time evolution of the Green's function governing $\langle c_2^\dagger(t+\tau)c_2(t)\rangle$ and the first cavity C_1's Purcell enhancement of the emitter barely changes due to addition of the second cavity C_2.[11]

EXPERIMENTAL DESIGN

Based on the parameter studies of the previous section, we propose a SiN-based nanophotonic structure achievable with current fabrication and experimental techniques to improve the indistinguishability of emitted photons from colloidal QDs. We observed in the last section that a mode volume of the first cavity between $0.1\left(\frac{\lambda}{n}\right)^3$ to $1\left(\frac{\lambda}{n}\right)^3$ is required to achieve optimal performance from our system. Based on the current state of art, on-substrate SiN cavities can achieve a mode volume of $\sim 1.2(\lambda/n)^3$, with a Q factor of $\sim 6 \times 10^4$ in a one-dimensional nanobeam structure (see Supporting Information). For the second cavity, we want a large Q_2, while the mode volume is not important. Hence, we can employ a SiN ring resonator with a quality factor $Q_2 = 2 \times 10^6$ for this purpose.[22,23] Finally, we want J to be slightly larger than γ and, hence, we choose $J = 2.1\gamma$. This can be engineered by appropriately choosing the distance between the two cavities.

As shown in the Figure 5a, our system consists of a colloidal QD coupled to a SiN nanobeam cavity, which is further coupled to a SiN ring resonator. The colloidal QD is characterized[10] by its decay time constant of $\tau = 4.8$ ns and a line width of $\Delta\lambda = 23$ nm, which can be used to find its decay rate γ and dephasing rate γ^*.

$$\gamma = \frac{1}{\tau}, \quad \gamma^* = \Delta\omega - \gamma, \quad \Delta\omega = \frac{\omega_o^2 \Delta\lambda}{2\pi c}$$

where ω_o is the emission frequency equivalent to $\lambda = 630$ nm. The QD is coupled to the nanobeam cavity with a coupling rate of g, which depends on the mode volume of the first cavity and the dipole moment of the QD and is given by[24,25]

$$g = \eta\sqrt{\frac{\mu^2\omega_o}{2\hbar\varepsilon_{sin}\varepsilon_o V_{eff}}}$$

where η is the relative strength of electric field at colloidal QD location (E_{CQD}/E_{max}) and is equal to 0.35 in our case,[10] as the QD sits on the surface of the cavity, μ denotes the dipole moment of the colloidal QD and is approximately 50D for the QD used.[26] The mode volume V_{eff} is calculated using[27−29]

$$V_{eff} = \frac{\int \varepsilon E^2 dV}{\max(\varepsilon E^2)}$$

A more general approach for calculating the mode volume of an optical cavity exists,[30] but for dielectric cavities with high Q factors, our method is also highly accurate.[31] The nanobeam cavity has a decay rate of $\kappa_1 = \omega_o/Q_1$ and is coupled to the ring resonator with a coupling rate $J = 2.1\gamma$. The ring resonator decays at a rate of $\kappa_2 = \omega_o/Q_2$. The QD radiates at $\lambda = 630$ nm and cavities are designed to have zero detuning. We pump the quantum dot with 3 ps pulse, which has an amplitude $P_o = 120\gamma$. Figure 5b shows a scanning electron microscope (SEM) of a fabricated concept device to highlight that such heterogeneous integration of different cavities is indeed possible.

Via numerically simulating the master equation using these parameters, we plot the population in the colloidal QD, the nanobeam and the ring resonator as a function of time (Figure 6). Initially, all three are in the ground state. As the pulse excites the emitter the population of QD rapidly rises before it starts to drop. Due to the coupling between the QD and the nanobeam, and the coupling between the nanobeam and the ring resonator, population in the cavities too show a similar behavior but with a decreasing magnitude of peak population. A key difference to note here from the case where we start with an initially excited emitter is that, since there exists a finite period of rise of populations, the net transfer to the second cavity (ring resonator) is lower in this case and we get a lower efficiency though indistinguishability is not significantly affected. We achieve an efficiency of 0.152% and indistinguishability of 0.629 using our system.

DOI: 10.1021/acsphotonics.9b01481
ACS Photonics XXXX, XXX, XXX−XXX

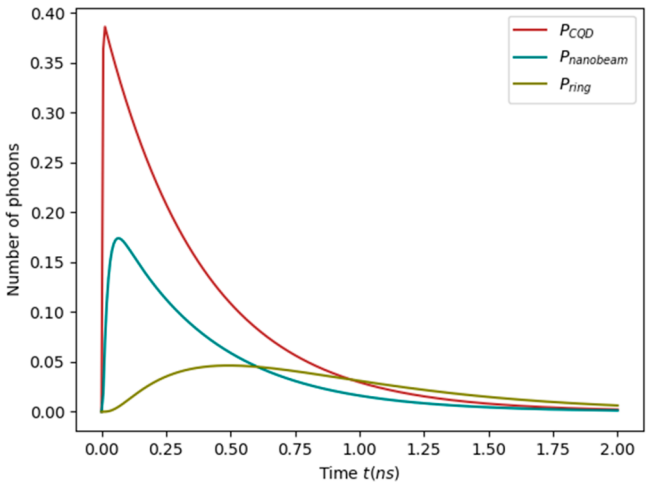

Figure 6. Population dynamics. We plot how the population of photons in the colloidal quantum dot, the nanobeam, and ring resonator, given by P_{CQD}, $P_{nanobeam}$, and P_{ring}, respectively, change with time. Population of the nanobeam has been multiplied by a factor 20 and the population of the ring resonator has been multiplied by a factor of 50. It is evident that such a process is not very efficient, but it ensures a high indistinguishability of photons collected from the ring resonator.

COMPARISON WITH OTHER SOLID-STATE EMITTERS

Finally, we compare the performance of colloidal QD as a source of indistinguishable single photons with other quantum emitters like self-assembled QDs and SiV centers. As seen from Table 1, colloidal QDs suffer from a dephasing rate that is almost 2 orders of magnitude greater than SiV centers and about 3 orders of magnitude greater than self-assembled QDs. The first column lists the indistinguishability and efficiency of a dissipative self-assembled QD coupled to a single cavity. Indistinguishability of such a system depends on the detuning between the cavity and the emitter and falls with an increase in detuning. The second column details the performance of a single SiV center coupled to system of cascaded cavities for two different parameter values. We can see that an increased indistinguishability comes at a cost of lower efficiency of emission. In the third column we list the performance of colloidal QD coupled to our proposed system of two cascaded cavities at an optimal point of operation. As evident, despite the huge amount of dephasing present in solution-processed colloidal QDs we can still get comparable indistinguishability and efficiency from these. However, as explained in the last section, current fabrication techniques pose limitations on the system parameters that can be presently achieved on a nanophotonic platform. Hence, in the last column, we list the performance of a colloidal QD coupled to our system of two coupled cavities characterized by parameters currently within the reach of experimental techniques. We can see that SiV centers yield high values of indistinguishability of emitted photons when coupled to a cavity with extremely low mode volume of the order of $\sim 0.005(\lambda/n)^3$. The caveat, however, is that such small mode volume cavities were only demonstrated on a high refractive index material platform, which is partially absorptive at the SiV resonance frequency.

CONCLUSION

We proposed an experimentally feasible system design to improve indistinguishability of single photons from colloidal QDs. We looked at the trends in indistinguishability and efficiency of emitted photons as a function of system parameters. Using qualitative arguments, we provided physical insight on how the system functions. Finally, we compared the performance of colloidal QDs with other broad quantum emitters. We found performance of colloidal QDs to be comparable to these other emitters. Even better performance from colloidal QD as a source of indistinguishable single photons is within reach in near future by using lower mode volume SiN cavities to couple to the colloidal QD. Another viable alternate is to use gallium phosphide (GaP) cavities as GaP has a much higher refractive index ($n = 3.25$). This high refractive index contrast allows significantly lower mode volumes of the order of $\sim 0.1(\lambda/n)^3$ to be achieved on a GaP-based nanophotonic platform. As shown in parameter sweeps and Table 1, using such low mode volumes in either platform, we can achieve indistinguishability greater than 0.9 using colloidal QDs. This number is expected to improve further, thanks to progress in synthesis techniques and new materials like Perovskite QDs.[33] Our work lays a solid foundation for obtaining indistinguishable photons from colloidal QDs coupled to a nanophotonic platform and can potentially solve the long-standing challenge of scalable quantum photonic technology.

ASSOCIATED CONTENT

Supporting Information

The Supporting Information is available free of charge on the ACS Publications website at DOI: 10.1021/acsphotonics.9b01481.

Table 1. Comparison between Performance of Broad Quantum Emitters: Self-Assembled QDs, SiV Centers, and Colloidal QDs, as Sources of Indistinguishable Single Photons under Incoherent Pumping[a]

category	self-assembled QD in a single cavity[13,32]	SiV center in coupled cavities[11]	colloidal QD in coupled cavities (optimal)	colloidal QD in coupled cavities (experimental)
γ^*/γ	117	2500	83000	83000
Q_1 and Q_2	$\sim 5 \times 10^4$	7×10^3 and $5 \times 10^5/3.6 \times 10^3$ and 5×10^4	6×10^4 and 2×10^6	6×10^4 and 2×10^6
V_{eff}	$\sim(\lambda/n)^3$	$0.007(\lambda/n)^3$	$0.1(\lambda/n)^3$	$1.2(\lambda/n)^3$
indistinguishability	~0.6	0.94/0.78	0.9	0.63
efficiency	12.1%	0.26%/0.99%	0.24%	0.15%

[a]Performance of SiV center has been listed for two sets of parameters taken from the cited paper. V_{eff} in the third row is the mode volume of the cavity to which the emitter is coupled. Note: results used for self-assembled QDs and SiV centers from the referenced papers have been updated to include the effect of pulsed incoherent pumping.

DOI: 10.1021/acsphotonics.9b01481
ACS Photonics XXXX, XXX, XXX−XXX

Detailed description of the mathematical framework used to model the device; Design parameters of the nanobeam cavity used in the device (PDF)

AUTHOR INFORMATION

Corresponding Author

*E-mail: arka@uw.edu.

ORCID

Abhi Saxena: 0000-0001-6453-929X

Yueyang Chen: 0000-0002-4390-550X

Arka Majumdar: 0000-0003-0917-590X

Notes

The authors declare no competing financial interest.

ACKNOWLEDGMENTS

This work is supported by NSF Award 1836500. A.S. is supported by a CEI graduate fellowship. A.R. is supported by the IC Postdoctoral Fellowship.

REFERENCES

(1) Rudolph, T. Why I Am Optimistic about the Silicon-Photonic Route to Quantum Computing. *APL Photonics* **2017**, *2* (3), No. 030901.

(2) Bogdanov, S.; Shalaginov, M. Y.; Boltasseva, A.; Shalaev, V. M. Material Platforms for Integrated Quantum Photonics. *Opt. Mater. Express* **2017**, *7* (1), 111.

(3) Takeda, S.; Furusawa, A. Toward Large-Scale Fault-Tolerant Universal Photonic Quantum Computing. *APL Photonics* **2019**, *4* (6), No. 060902.

(4) Knill, E.; Laflamme, R.; Milburn, G. J. A Scheme for Efficient Quantum Computation with Linear Optics. *Nature* **2001**, *409* (6816), 46.

(5) Kimble, H. J. The Quantum Internet. *Nature* **2008**, *453* (7198), 1023−1030.

(6) Spring, J. B.; Metcalf, B. J.; Humphreys, P. C.; Kolthammer, W. S.; Jin, X.-M.; Barbieri, M.; Datta, A.; Thomas-Peter, N.; Langford, N. K.; Kundys, D.; et al. Boson Sampling on a Photonic Chip. *Science* **2013**, *339* (6121), 798−801.

(7) Senellart, P.; Solomon, G.; White, A. High-Performance Semiconductor Quantum-Dot Single-Photon Sources. *Nat. Nanotechnol.* **2017**, *12* (11), 1026−1039.

(8) Hoang, T. B.; Akselrod, G. M.; Mikkelsen, M. H. Ultrafast Room-Temperature Single Photon Emission from Quantum Dots Coupled to Plasmonic Nanocavities. *Nano Lett.* **2016**, *16* (1), 270−275.

(9) Santori, C.; Fattal, D.; Vučković, J.; Solomon, G. S.; Yamamoto, Y. Indistinguishable Photons from a Single-Photon Device. *Nature* **2002**, *419* (6907), 594−597.

(10) Chen, Y.; Ryou, A.; Friedfeld, M. R.; Fryett, T.; Whitehead, J.; Cossairt, B. M.; Majumdar, A. Deterministic Positioning of Colloidal Quantum Dots on Silicon Nitride Nanobeam Cavities. *Nano Lett.* **2018**, *18* (10), 6404−6410.

(11) Choi, H.; Zhu, D.; Yoon, Y.; Englund, D. Cascaded Cavities Boost the Indistinguishability of Imperfect Quantum Emitters. *Phys. Rev. Lett.* **2019**, *122* (18), 183602.

(12) Sun, F. W.; Wong, C. W. Indistinguishability of Independent Single Photons. *Phys. Rev. A: At., Mol., Opt. Phys.* **2009**, *79* (1), No. 013824.

(13) Grange, T.; Hornecker, G.; Hunger, D.; Poizat, J.-P.; Gérard, J.-M.; Senellart, P.; Auffèves, A. Cavity-Funneled Generation of Indistinguishable Single Photons from Strongly Dissipative Quantum Emitters. *Phys. Rev. Lett.* **2015**, *114* (19), 193601.

(14) Lanco, L.; Senellart, P. A Highly Efficient Single Photon-Single Quantum Dot Interface. In *Engineering the Atom-Photon Interaction: Controlling Fundamental Processes with Photons, Atoms and Solids*, Nano-Optics and Nanophotonics; Predojević, A., Mitchell, M. W., Eds.; Springer International Publishing: Cham, 2015; pp 39−71, DOI: 10.1007/978-3-319-19231-4_2.

(15) Berthelot, A.; Favero, I.; Cassabois, G.; Voisin, C.; Delalande, C.; Roussignol, Ph.; Ferreira, R.; Gérard, J. M. Unconventional Motional Narrowing in the Optical Spectrum of a Semiconductor Quantum Dot. *Nat. Phys.* **2006**, *2* (11), 759−764.

(16) Wein, S.; Lauk, N.; Ghobadi, R.; Simon, C. Feasibility of Efficient Room-Temperature Solid-State Sources of Indistinguishable Single Photons Using Ultrasmall Mode Volume Cavities. *Phys. Rev. B: Condens. Matter Mater. Phys.* **2018**, *97* (20), 205418.

(17) Breuer, H.-P.; Petruccione, F.; Petruccione, S. *The Theory of Open Quantum Systems*; Oxford University Press, 2002.

(18) Gardiner, C.; Zoller, P.; Zoller, P. *Quantum Noise: A Handbook of Markovian and Non-Markovian Quantum Stochastic Methods with Applications to Quantum Optics*; Springer Science & Business Media, 2004.

(19) Englund, D.; Majumdar, A.; Faraon, A.; Toishi, M.; Stoltz, N.; Petroff, P.; Vučković, J. Resonant Excitation of a Quantum Dot Strongly Coupled to a Photonic Crystal Nanocavity. *Phys. Rev. Lett.* **2010**, *104* (7), No. 073904.

(20) Johansson, J. R.; Nation, P. D.; Nori, F. QuTiP: An Open-Source Python Framework for the Dynamics of Open Quantum Systems. *Comput. Phys. Commun.* **2012**, *183* (8), 1760−1772.

(21) Auffèves, A.; Gerace, D.; Gérard, J.-M.; Santos, M. F.; Andreani, L. C.; Poizat, J.-P. Controlling the Dynamics of a Coupled Atom-Cavity System by Pure Dephasing. *Phys. Rev. B: Condens. Matter Mater. Phys.* **2010**, *81* (24), 245419.

(22) Hosseini, E. S.; Yegnanarayanan, S.; Atabaki, A. H.; Soltani, M.; Adibi, A. High Quality Planar Silicon Nitride Microdisk Resonators for Integrated Photonics in the VisibleWavelength Range. *Opt. Express* **2009**, *17* (17), 14543−14551.

(23) Gondarenko, A.; Levy, J. S.; Lipson, M. High Confinement Micron-Scale Silicon Nitride High Q Ring Resonator. *Opt. Express* **2009**, *17* (14), 11366.

(24) McCutcheon, M. W.; Loncar, M. Design of a Silicon Nitride Photonic Crystal Nanocavity with a Quality Factor of One Million for Coupling to a Diamond Nanocrystal. *Opt. Express* **2008**, *16* (23), 19136.

(25) Barclay, P. E. Fiber-Coupled Nanophotonic Devices for Nonlinear Optics and Cavity QED. *Ph.D. Thesis*, California Institute of Technology, 2007.

(26) Kortschot, R. J.; van Rijssel, J.; van Dijk-Moes, R. J. A.; Erné, B. H. Equilibrium Structures of PbSe and CdSe Colloidal Quantum Dots Detected by Dielectric Spectroscopy. *J. Phys. Chem. C* **2014**, *118* (13), 7185−7194.

(27) Choi, H.; Heuck, M.; Englund, D. Self-Similar Nanocavity Design with Ultrasmall Mode Volume for Single-Photon Nonlinearities. *Phys. Rev. Lett.* **2017**, *118* (22), 223605.

(28) Gupta, S.; Waks, E. Spontaneous Emission Enhancement and Saturable Absorption of Colloidal Quantum Dots Coupled to Photonic Crystal Cavity. *Opt. Express* **2013**, *21* (24), 29612.

(29) Kristensen, P. T.; Vlack, C. V.; Hughes, S. Generalized Effective Mode Volume for Leaky Optical Cavities. *Opt. Lett.* **2012**, *37* (10), 1649−1651.

(30) Sauvan, C.; Hugonin, J. P.; Maksymov, I. S.; Lalanne, P. Theory of the Spontaneous Optical Emission of Nanosize Photonic and Plasmon Resonators. *Phys. Rev. Lett.* **2013**, *110* (23), 237401.

(31) Srinivasan, K.; Barclay, P. E.; Borselli, M.; Painter, O. Optical-Fiber-Based Measurement of an Ultrasmall Volume High-Q Photonic Crystal Microcavity. *Phys. Rev. B: Condens. Matter Mater. Phys.* **2004**, *70* (8), 081306.

(32) Arakawa, Y.; Iwamoto, S.; Nomura, M.; Tandaechanurat, A.; Ota, Y. Cavity Quantum Electrodynamics and Lasing Oscillation in Single Quantum Dot-Photonic Crystal Nanocavity Coupled Systems. *IEEE J. Sel. Top. Quantum Electron.* **2012**, *18* (6), 1818−1829.

(33) Utzat, H.; Sun, W.; Kaplan, A. E. K.; Krieg, F.; Ginterseder, M.; Spokoyny, B.; Klein, N. D.; Shulenberger, K. E.; Perkinson, C. F.; Kovalenko, M. V.; Bawendi, M. G. Coherent Single-Photon Emission

DOI: 10.1021/acsphotonics.9b01481
ACS Photonics XXXX, XXX, XXX−XXX

from Colloidal Lead Halide Perovskite Quantum Dots. *Science* **2019**, *363*, 1068.

DOI: 10.1021/acsphotonics.9b01481
ACS Photonics XXXX, XXX, XXX−XXX